

1 **Lithium isotopes in speleothems: Temperature-controlled variation in**  
2 **silicate weathering during glacial cycles**

3

4 Philip A.E. Pogge von Strandmann<sup>1,2</sup>, Anton Vaks<sup>2,3</sup>, Miryam Bar-Matthews<sup>3</sup>,  
5 Avner Ayalon<sup>3</sup>, Ezekiel Jacob<sup>2</sup>, and Gideon M. Henderson<sup>2</sup>

6

7 <sup>1</sup>London Geochemistry and Isotope Centre (LOGIC), Institute of Earth and  
8 Planetary Sciences, University College London and Birkbeck, University of  
9 London, Gower Street, London, WC1E 6BT, UK.

10 <sup>2</sup>Department of Earth Sciences, University of Oxford, South Parks Road, Oxford,  
11 UK.

12 <sup>3</sup>Geological Survey of Israel, 30 Malkhey Israel Street, 9550161 Jerusalem, Israel.

13

14

15 Abstract

16 Terrestrial chemical weathering of silicate minerals is a fundamental component  
17 of the global cycle of carbon and other elements. Past changes in temperature,  
18 rainfall, ice cover, sea-level and physical erosion are thought to affect weathering  
19 but the relative impact of these controls through time remains poorly  
20 constrained. This problem could be addressed if the nature of past weathering  
21 could be constrained at individual sites. In this study, we investigate the use of  
22 speleothems as local recorders of the silicate weathering proxy, Li isotopes. We  
23 analysed  $\delta^7\text{Li}$  and [Li] in speleothems that formed during the past 200 ka in two  
24 well-studied Israeli caves (Soreq and Tzavoa), as well as in the overlying soils  
25 and rocks. Leaching and mass balance of these soils and rocks show that Li is  
26 dominantly sourced from weathering of the overlying aeolian silicate soils.

27 Speleothem  $\delta^7\text{Li}$  values are ubiquitously higher during glacials ( $\sim 23\text{‰}$ ) than  
28 during interglacials ( $\sim 10\text{‰}$ ), implying more congruent silicate weathering  
29 during interglacials (where “congruent” means a high ratio of primary mineral  
30 dissolution to secondary mineral formation). These records provide information  
31 on the processes controlling weathering in Israel. Consideration of possible  
32 processes causing this change of weathering congruency indicates a primary role  
33 for temperature, with higher temperatures causing more congruent weathering  
34 (lower  $\delta^7\text{Li}_{\text{speleo}}$ ). The strong relationship observed between speleothem  $\delta^7\text{Li}$   
35 and climate at these locations suggests that Li isotopes may be a powerful tool  
36 with which to understand the local controls on weathering at other sites, and  
37 could be used to assess the distribution of weathering changes accompanying  
38 climate change, such as that of Pleistocene glacial cycles.

39

40 Keywords: weathering; glaciation; climate; lithium isotopes; temperature.

41

## 42 1.0 Introduction

43 Weathering of silicate minerals is a fundamental aspect of the global cycle  
44 of carbon and other elements and plays an important role in moderating climate  
45 and controlling ocean chemistry on long timescales. Controls on the rate and  
46 style of weathering include temperature, rainfall and the supply of fresh silicate  
47 material (West et al., 2005), but separating the relative importance of these  
48 controls over geological time has been challenging (Archer et al., 2000; Foster  
49 and Vance, 2006).

50 The major climate changes of Pleistocene glacial cycles likely caused  
51 changes in weathering at different scales, but are an example of the lack of  
52 adequate understanding of past weathering, with various studies predicting that

53 CO<sub>2</sub> drawdown by silicate weathering was between ~6–20% lower (Ludwig et  
54 al., 1999; Mokadem et al., 2015; Munhoven, 2002) to 250% higher (Munhoven  
55 and Francois, 1996) during the Last Glacial Maximum (LGM) than at present.  
56 Perhaps the most widely used proxy for weathering, seawater radiogenic  
57 strontium, shows no direct evidence for changing weathering during these  
58 cycles, but provides limits on maximum possible changes at a global scale  
59 (Mokadem et al., 2015; Vance et al., 2009). Similarly, studies based on Be  
60 isotopes suggest little variation in silicate weathering rates between glacial and  
61 interglacial states (von Blanckenburg et al., 2015), similar to some carbon mass  
62 balance calculations (Zeebe and Caldeira, 2008). However, it is also clear that  
63 weathering varied dramatically at the local scale on these timescales, due to  
64 different impacts by temperature, glacial grinding and sealevel changes (Frings  
65 et al., 2016). Studies of Pb isotopes in Fe-Mn crusts offshore the Laurentide ice  
66 sheet have allowed a more local approach, and suggest that chemical weathering  
67 was significantly (~2–3 times) lower during glacials than interglacials in this  
68 glaciated region (Crocket et al., 2013; Foster and Vance, 2006). Equally,  
69 authigenic phases from the Indian Ocean suggest that Himalayan weathering was  
70 up to 5 times lower during glacials (Wilson et al., 2015). Neodymium isotopes  
71 have been similarly interpreted, suggesting that Himalayan river discharge and  
72 weathering was lower in glacials (Burton and Vance, 2000; Gourlan et al., 2010).  
73 In contrast, Nd isotopes from around New Zealand suggest that weathering  
74 increased 2–10 times during glacials, due to the proximity of physically eroded  
75 material from glaciers (Cogez et al., 2015). Similarly, records from the South  
76 China Sea suggest elevated weathering fluxes during glacials due to greater  
77 continental exposure during sea-level fall (Wan et al., 2017). There is potential  
78 ambiguity in some of these interpretations, because radiogenic isotopes are

79 largely controlled by weathering provenance, and often cannot distinguish  
80 between weathering of silicates and carbonates. Such marine studies are also  
81 only able to assess past weathering at a limited range of locations and  
82 geographical scales. The ability to assess past weathering for particular  
83 environments from local continental records would be a powerful addition to the  
84 range of tools used to assess past weathering. Lithium isotopes are a tracer for  
85 weathering that respond solely to silicate weathering. Lithium is enriched in  
86 silicates by a factor of  $\sim 10^3$ – $10^4$  relative to crustal carbonates, so that, even in  
87 carbonate catchments, Li is dominated by weathering of silicate rocks (Kisakürek  
88 et al., 2005). Further, Li isotopes are not fractionated by plants or primary  
89 productivity (Pogge von Strandmann et al., 2016). The  $\delta^7\text{Li}$  of primary silicate  
90 rocks defines a narrow range ( $\sim 0$ – $5\text{‰}$ , Teng et al., 2004), and the high  
91 variability of  $\delta^7\text{Li}$  in modern rivers and soil pore fluids ( $2$ – $42\text{‰}$ ; global mean  
92  $\sim 23\text{‰}$ , (Dellinger et al., 2015; Huh et al., 1998; Pogge von Strandmann and  
93 Henderson, 2015) is due to preferential uptake of  $^6\text{Li}$  by secondary clay minerals  
94 (e.g. phyllosilicates) during the weathering process (Pistiner and Henderson,  
95 2003). The  $\delta^7\text{Li}$  of surface water is therefore controlled by the “weathering  
96 congruency”, defined here (as is now common for Li isotope studies) as the ratio  
97 of primary mineral dissolution to secondary mineral formation, with congruent  
98 weathering leading to low  $\delta^7\text{Li}$  (Dellinger et al., 2015; Pogge von Strandmann et  
99 al., 2017; Pogge von Strandmann and Henderson, 2015). Fully congruent  
100 weathering has never been observed, and rock-like  $\delta^7\text{Li}$  values tend to only occur  
101 in hydrothermal waters where clay formation is limited (Pogge von Strandmann  
102 et al., 2016). Dissolved  $\delta^7\text{Li}$  might also be affected by re-dissolving (isotopically  
103 light) secondary minerals, although to date this has only been reported to affect

104  $\delta^7\text{Li}$  in rainforest catchments with very different weathering regimes from those  
105 observed here (Clergue et al., 2015; Dellinger et al., 2015).

106 Lithium isotopes have been used to assess possible changes in weathering  
107 globally, though measurement of seawater carbonates (Hathorne and James,  
108 2006; Lechler et al., 2015). They may also be a powerful tracer of local changes  
109 and the processes controlling weathering if a suitable substrate to record their  
110 variation is identified. In this study, we assess the use of speleothems (cave  
111 carbonates) as recorders of  $\delta^7\text{Li}$  to provide a local record of terrestrial silicate  
112 weathering through time. Speleothems are an archive for high-resolution  
113 examination of past environmental conditions. In particular, speleothem  
114 chemistry is determined largely by drip water chemistry (Bar-Matthews et al.,  
115 1999; Vaks et al., 2006), which in turn is dominated by weathering processes  
116 occurring immediately above the cave (Ayalon et al., 1999). We have examined Li  
117 isotope ratios in speleothems from two well-studied Israeli caves, Soreq and  
118 Tzavoa, which are located in very different climate regimes: sub-humid  
119 Mediterranean and mildly-arid semi-desert climate, respectively.

120

## 121 2.0 Field area

122 Speleothems from two caves in Israel were examined: Soreq is on the  
123 western slope of the Judean Mountains, ~20 km west of Jerusalem, while Tzavoa  
124 is in the northern Negev Desert, which is a part of a larger Saharan-Arabian  
125 Desert belt (Fig. 1). A detailed description of the climate and environment of  
126 these caves is important, because it allows us to examine the precise weathering  
127 environments.

128

## 129 *2.1 Climate setting*

130 Soreq is located in a sub-humid Mediterranean climate, while Tzavoa is in  
131 mildly arid desert 65 km to the south-east, with a zone of semi-arid steppe  
132 between the two caves (Fig. 1C). Soreq Cave currently experiences 500 mm/yr  
133 rain, with a 19.5°C Average Annual Temperature (AAT), while Tzavoa  
134 experiences 150 mm/yr rain, with an AAT of 18.5°C, because of higher altitude  
135 (500-550m above sea-level) than Soreq (400m). During the last glacial, the  
136 temperatures in the region were 5–10°C lower than today (Affek et al., 2008;  
137 Almogi-Labin et al., 2009; McGarry et al., 2004). Higher  
138 precipitation/evaporation ratios during the last two glacial intervals led to  
139 intensive speleothem deposition in Tzavoa Cave (Vaks et al., 2006), but lack of  
140 moisture during most of interglacials led to limited interglacial speleothem  
141 deposition occurring only during Marine Isotopic Stages (MIS)-7a, MIS-5e and  
142 MIS-5a. In contrast, speleothem deposition at Soreq is fairly continuous  
143 throughout the studied time period (Bar-Matthews et al., 2003).

144 The major rainfall source is mid-latitude Atlantic–Mediterranean cyclones  
145 moving eastwards above the eastern Mediterranean Sea. The northern Sinai  
146 coastline therefore forms the southern limit at which rainclouds usually form,  
147 and the latter are carried to the east, leaving the southern region dry. This  
148 phenomenon causes the sharp precipitation gradient between Soreq Cave  
149 (central Israel) and Tzavoa Cave (northern Negev Desert), although the distance  
150 between them is only 65 km.

151

## 152 *2.2 Cave settings – geology and vegetation*

153 Soreq and Tzavoa caves are found within dolomites and limestones of the  
154 Upper Cretaceous Judea Group. The caves were likely formed between the Late  
155 Eocene and Miocene when the Judea Group was below the groundwater table.

156 The caves were uplifted above the groundwater table during two major tectonic  
157 phases in the Late Miocene–Pliocene, and during the Early Pleistocene (Frumkin  
158 and Fischhendler, 2005; Vaks et al., 2013b), into the unsaturated zone that  
159 enabled the formation of vadose speleothems.

160 The vegetation above Soreq Cave is Mediterranean maquis with low trees,  
161 bushes, shrubs and grasses, covering 50–80% of the surface (Fig. 2a). Above  
162 Tzavoa the vegetation is Irano-Turanian semi-desert grasses and shrubs  
163 covering less than 20% of the surface (Fig. 2c). Both caves are located on the  
164 slopes of mountains with relatively steep relief above the caves (5–45°, with  
165 occasional small cliffs), whereas small horizontal/moderate relief areas are  
166 found on the topographic highs above the caves.

167

### 168 *2.3 Soils*

169 The soil above the Soreq cave is of Mediterranean Terra-Rosa type, while  
170 above Tzavoa Cave it is of Loess type. Both soils appear as isolated pockets up to  
171 few tens of cm in depth between rock outcrops. Local soils are largely aeolian in  
172 origin, from dust transported from the Saharan Desert and nearer Northern Sinai  
173 Sand Dune Field (originating from Nile river sediments), both to the south and  
174 west of the studied caves (Crouvi et al., 2007) (Fig. 1b). Atlantic-Mediterranean  
175 cyclones transport this dust from its source into Israel, with dust fall ~100–130  
176 g/m<sup>2</sup>/yr at the cave sites (Fig. 1b) (Ganor and Foner, 2001). During the last two  
177 glacial periods the research area received more dust compared to today because  
178 of the exposure of large areas of the Nile delta (Amit et al., 2011; Enzel et al.,  
179 2008), expansion of the Saharan-Arabian desert belt (Frumkin and Stein, 2004)  
180 and higher intensity SWW winds (Enzel et al., 2008). The primary mineralogy of  
181 Israeli soils in both regions tends to be similar, with around 30–40% quartz, 20–

182 30% calcite, ~8% K-feldspar and 7–10% plagioclase, with the remainder largely  
183 made up by fine-grained phyllosilicates (Ben-Israel et al., 2015; Crouvi et al.,  
184 2009; Sandler et al., 2015). The clay fraction at the two locations is slightly  
185 different, with Soreq dominated by illite-smectite clays (~80%) and 10–15%  
186 kaolinite, while Tzavoa consists of ~70% illite-smectite and 20–30% kaolinite  
187 (Sandler, 2013; Sandler et al., 2015).

188 At least 50% of the Mediterranean Terra-Rosa soil is aeolian (Yaalon,  
189 1997), whereas the loess soils in the Negev are entirely aeolian (Crouvi et al.,  
190 2010). OSL ages of Terra-Rosa soils ~10 km to the east of Soreq Cave show that  
191 their age varies from 180–9000 years (Gadot et al., 2016), whereas the age of the  
192 loess soils in the Negev desert (Tzavoa Cave location) is 10–14 ka (Crouvi et al.,  
193 2009; Faershtein et al., 2016). The evidence therefore indicates that residence  
194 time of the soil cover (in pockets of <50 cm in depth) above Soreq Cave is less  
195 than ~10 ka, and the residence time of the thin loess soil pockets (0–15 cm)  
196 above the Tzavoa Cave is less than ~14 ka.

197

### 198 3.0 Methods

199 Speleothem samples were initially dissolved in 1M HCl, and trace element  
200 concentrations were analysed using a Thermo Scientific Element 2 ICP-MS  
201 (inductively coupled plasma mass spectrometer), by calibrating with a series of  
202 multi-element solutions. Accuracy and precision were assessed by analysis of the  
203 international reference standard JLS-1, and was within  $\pm 4\%$  for major elements  
204 and  $\pm 6\%$  for Li concentrations.

205 Most of the speleothems' chronology was based on previous studies (Bar-  
206 Matthews et al., 2003; Grant et al., 2012; Vaks et al., 2006). To refine the age

207 model of one speleothem's layer, 2-22-1<sub>2</sub>, a single U-Th age determination was  
208 performed according to the method described in Vaks et al., 2013a).

209 Soils were sequentially leached by the Tessier method adapted by Pogge  
210 von Strandmann et al. (2013). The exchangeable fraction was extracted using 1M  
211 Na-acetate (NaOAc), and the carbonate fraction in 1M NaOAc adjusted to pH5  
212 with acetic acid. The final silicate fraction (as well as the bulk rock) was  
213 dissolved in a standard routine of HF-HNO<sub>3</sub>-HClO<sub>4</sub>, followed by HNO<sub>3</sub> and HCl.

214 Following determination of [Li], between 0.05–0.25g of speleothem were  
215 dissolved in weak HCl to minimise leaching of any minor silicates in the  
216 speleothems. The amount of material dissolved was initially targeted to gain  
217 ~15ng Li, but following the use of a new-geometry cone (Le Roux, 2010), only  
218 ~5ng Li were needed. This dissolution was also analysed for trace elements by  
219 ICP-MS, specifically Al/Ca and Mn/Ca, to assess whether any silicates had been  
220 leached during dissolution. The cutoff for Al/Ca in carbonates has been  
221 calculated at 0.8 mmol/mol (Pogge von Strandmann et al., 2013), although  
222 values in this study were <0.07 mmol/mol. Li/Ca was also analysed, to compare  
223 the leaches to the 1M HCl dissolutions. There was agreement between these two  
224 Li content analyses within analytical uncertainty, demonstrating that silicates  
225 were not significantly leached during the initial HCl dissolution used for  
226 concentration analyses.

227

### 228 *3.1 Lithium chemistry and analyses*

229 Speleothems have low Li/Ca ratios, so a new Li isotope chemistry was  
230 developed to deal with the large amount of carbonate matrix. This was based on  
231 a scaled-up version of the weak HCl elution technique (Pogge von Strandmann et  
232 al., 2013). The first column consisted of 20ml AG50W-X12, where Li was eluted

233 in 1M HCl. This column separated Li from Ca, but not from Na. The second  
234 column is identical to that used in Pogge von Strandmann et al., 2013, and  
235 consisted of 1ml AG50W X-12, with Li eluted in 0.2M HCl. Leached and silicate  
236 fractions were purified by the standard 2-column method detailed elsewhere  
237 (Pogge von Strandmann and Henderson, 2015; Pogge von Strandmann et al.,  
238 2013). Given that Li isotopes are fractionated during ion chromatography, yields  
239 were tested by collecting splits before and after the Li collection bracket. Results  
240 showed that <0.1% of Li was present in these splits, suggesting that close to  
241 100% was in the fraction collected for analysis. The total procedural blank for Li  
242 isotope analysis is ~0.02–0.05ng Li, which is insignificant compared to sample Li.

243         Analyses were performed on a Nu Plasma HR multi-collector ICP-MS at  
244 Oxford University, using a sample-standard bracketing system relative to the  
245 LSVEC standard. Analysis methods were identical to those described in Pogge  
246 von Strandmann and Henderson (2015). At an uptake rate of 75  $\mu\text{l}/\text{min}$ , the  
247 sensitivity for a 20 ng/ml solution is ~23 pA of  $^7\text{Li}$  using a standard type “A”  
248 cone, and  $10^{-11}$   $\Omega$  resistors. When using the new-geometry skimmer cone (“low-  
249 mass high-abundance” cone (Le Roux, 2010)), 5ng/ml solution gives a  $^7\text{Li}$  beam  
250 intensity of ~30pA for the same uptake rate, with a ~1.5 $\times$  improved signal to  
251 noise ratio. A drawback of the high-intensity cone is that it is more susceptible to  
252 matrix contributions, and therefore if sample Na/Li >1.5, the samples had to be  
253 repurified (with standard cones, Na/Li <3 is acceptable).

254         Accuracy and external reproducibility, as assessed from seawater and  
255 USGS standards BCR-2 and SGR-1, is  $31.3\pm 0.6\text{‰}$  (2sd, n=59, chemistry=59),  
256  $2.7\pm 0.4\text{‰}$  (n = 4, chemistry = 4) and  $3.6\pm 0.4\text{‰}$  (n=3, chemistry=3), respectively  
257 (where “chemistry” denotes separate passes through full purification chemistry),  
258 which agrees well with other studies (Dellinger et al., 2015; Phan et al., 2016;

259 Pogge von Strandmann and Henderson, 2015). Standards measured using the  
260 new cones and the larger first column were identical to those processed using  
261 the standard method. Precision was also assessed from repeated analyses  
262 (including leaching and chemistry) of our in-house marl standard, which also  
263 gives a reproducibility of  $\pm 0.6\text{‰}$  ( $n=9$ ) (Pogge von Strandmann et al., 2013).

264

## 265 4.0 Results

### 266 *4.1 Rocks and soils*

267 All rock and soil data from cave regions are given in Table 1 and show  
268 somewhat similar behaviour. The carbonate portion of the host rocks (i.e.  
269 leached fraction) have  $\delta^7\text{Li}$  values of 22.3 and 20.1‰ for Soreq and Tzavoa,  
270 respectively. In contrast, the silicate portion of the rocks have  $\delta^7\text{Li}$  values of 10.2  
271 and 6.1‰, respectively. The silicate portion of these carbonate rocks contains  
272 95–96% of the bulk rock Li, but only comprise 1.7–3.3% of the rock by mass.

273 The exchangeable fractions of the soils overlying the rocks contain  
274  $\sim 0.04\%$  of the total soil Li in both caves, and have  $\delta^7\text{Li}$  of 11.9–13.5‰. The  
275 carbonate fractions of the soils contain 0.04–0.13% of the total soil Li, and have  
276  $\delta^7\text{Li}$  values of 13.4–15.7‰, in keeping with the isotopically heavy compositions  
277 of marine-derived carbonate rocks. The silicate fractions in these soils contain  
278  $>99.8\%$  of the soil's Li, and have typical silicate rock  $\delta^7\text{Li}$  values of 1.6–2.5‰.

279

### 280 *4.2 Modern drip waters and precipitates*

281 Modern drip waters from both Soreq and Tzavoa were collected in 2014.  
282 These have relatively low Li concentrations (0.45–1.66 ng/ml), and  
283 concentrations do not correlate with the observed drip rates. Lithium isotope

284 ratios are similar for all the drip waters in both caves, ranging from 20.3 to  
285 23.9‰ (Supplementary table). In particular, drip waters were collected that are  
286 dripping onto recent cave carbonates precipitated onto concrete paths from the  
287 1970s in Soreq cave. These drip waters have  $\delta^7\text{Li}$  values of 22.8 to 23.9‰, 3.6–  
288 5.2‰ higher than the “speleothem” carbonate that is precipitating from them  
289 ( $\delta^7\text{Li} = 18.7\text{--}19.2\text{‰}$  – Fig. 3). This fractionation factor is identical to that  
290 reported from inorganic calcite experiments, which also reported that  
291 fractionation is not dependent on temperature (Marriott et al., 2004).

292

### 293 *4.3 Speleothems*

294 Eleven well-dated speleothems from Soreq Cave and four speleothems  
295 from Tzavoa Cave, which cover the past 200 kyr, were studied, and display  
296 strong glacial-interglacial variability in oxygen and carbon stable isotope and  
297 trace element concentrations (Ayalon et al., 1999; Bar-Matthews et al., 2003;  
298 Vaks et al., 2006). Lithium concentrations range from 24 to 470 ng/g, and tend to  
299 be higher but more variable during glacials (Fig. 4a).

300 Speleothems from the two caves show similar  $\delta^7\text{Li}$  behaviour, with a clear  
301 trend of higher  $\delta^7\text{Li}$  during glacials, and lower  $\delta^7\text{Li}$  during interglacials (Fig. 5).  
302 Soreq provides the most complete record, with speleothem  $\delta^7\text{Li}$  values reaching  
303 a peak of  $\sim 21\text{--}23\text{‰}$  during the maxima of the last two glaciations, minima of  
304  $9.8\text{‰}$  in the Holocene, and  $14.9\text{‰}$  in the penultimate deglacial.

305 Due to lack of interglacial moisture during the last 200 ka, Tzavoa Cave  
306 has limited speleothem deposition, occurring mainly during glacials, and only in  
307 some interglacials (MIS-7a, MIS-5e and MIS-5a). Just before the penultimate

308 glaciation,  $\delta^7\text{Li}$  values are  $\sim 15\text{‰}$ , and, in both glacials, isotope ratios increase to  
309  $\sim 23\text{‰}$ .

310 In the time periods when speleothems exist concurrently in both caves  
311 (14–76 ka, and 125–168 ka), the  $\delta^7\text{Li}$  values are generally within  $1\text{‰}$  of each  
312 other. At  $\sim 125\text{--}137$  ka, though,  $\delta^7\text{Li}$  values from Tzavoa are  $\sim 4\text{‰}$  lower, and at  
313 76 ka  $\sim 7\text{‰}$  higher than those in Soreq. Isotopic fractionation between calcite  
314 and solution observed here ( $3.6\text{--}5.2\text{‰}$  – see above) and experimentally ( $\sim 3\text{--}$   
315  $5\text{‰}$ ) (Marriott et al., 2004) (Fig. 3), suggest drip water  $\delta^7\text{Li}$  varied between  
316  $\sim 14\text{‰}$  shortly ( $\sim 15\text{kyr}$ ) after the glacial maxima, to  $\sim 27\text{‰}$  during glacials.

317

## 318 5.0 Discussion

### 319 *5.1 Modern drip waters and carbonates*

320 An aberration to the trend of decreasing  $\delta^7\text{Li}_{\text{speleo}}$  of the last 20,000 years  
321 (Fig. 5) is modern carbonate precipitated onto concrete paths. At the time of the  
322 youngest speleothem sample, 1,700 years ago, drip waters had a  $\delta^7\text{Li}$  of  $\sim 14\text{‰}$   
323 (assuming a calcite fractionation factor of  $4\text{‰}$  (Marriott et al., 2004)), while  
324 modern drip waters have values closer to  $22\text{‰}$ . Modern drip waters are  
325 enriched in K and  $\text{NO}_3$ , indicative of the effect of sewage, fertiliser (Orland et al.,  
326 2014) or industry contamination. Regional agriculture has increased  
327 significantly over the past 50–100 years (Orland et al., 2014). The modern  
328 carbonates have [Li] up to an order of magnitude higher than the 1,700 years old  
329 speleothem (Supplementary table), and fertilisers tend to be high in Li  
330 (Kisakürek et al., 2005). It is therefore probable that the modern samples have  
331 been contaminated by anthropogenic inputs, as also indicated by elevated  $\delta^{13}\text{C}$   
332 ratios (Ayalon et al., 1999; Bar-Matthews et al., 1999). Modern drip waters and

333 carbonates allow us, however, to confirm that the Li isotope fractionation into  
334 calcite in caves is similar to that in precipitation experiments (Fig. 3), but their  
335  $\delta^7\text{Li}_{\text{speleo}}$  values are likely not representative of the trends that characterise the  
336 rest of the 200 ka record.

337

### 338 *5.2 Negligible input of seawater Li*

339 Seawater is a significant contributor to the composition of Israeli  
340 rainwater (Mamane, 1987). The relative amount of contribution varies according  
341 to the element of interest and the location. Sodium is considered to be mainly  
342 sea-salt derived, and therefore Li/Na ratios of modern rainwater and  
343 speleothems can be used to determine whether significant amounts of Li have  
344 been sourced from sea-salt. Using published annual ranges for local rainwater Na  
345 concentrations ( $\sim 5.3\text{--}8.1\ \mu\text{g}/\text{ml}$  (Mamane, 1987; Mamane et al., 1987)), and our  
346 analysis of modern rain at Soreq ( $[\text{Li}] = 43\ \text{pg}/\text{ml}$ ), Li/Na mass ratios vary  
347 between  $5.4 \times 10^{-6}$  and  $8.2 \times 10^{-6}$  (seawater Li/Na =  $16.5 \times 10^{-6}$ ). Speleothem Li/Na  
348 therefore suggests that  $1.5 \pm 0.7\ \text{ng}/\text{g}$  of speleothem Li stems from rainwater  
349 ( $3.0 \pm 1.3\ \text{ng}/\text{g}$  if the seawater ratio were transferred to rainwater), which is  
350 insignificant compared to the speleothem Li concentrations of 25–470 ng/g.  
351 Speleothems with the lowest  $[\text{Li}]$  also tend to have low  $\delta^7\text{Li}$ , whereas seawater  
352 has high  $\delta^7\text{Li} = 31\text{‰}$ , further suggesting little sea-salt influence on speleothem Li  
353 compositions.

354

### 355 *5.3 Source of Li: soils*

356 The sequential leaching of the soils and host rocks showed that the  
357 exchangeable and carbonate fractions are isotopically heavy and have similar

358  $\delta^7\text{Li}$  values in comparable phases. The silicate (residue) fractions in the soil  
359 accounted for >99% of Li in the bulk soils, and had a  $\delta^7\text{Li} \sim 1.6\text{--}2.5\text{‰}$ , while the  
360 silicate fraction in the host carbonate rock accounted for >95% of the rocks' Li,  
361 with a  $\delta^7\text{Li}$  of 6–10‰ (Table 1). A simple mass balance can be used to calculate  
362 the ratio of Li contained in carbonates and silicates above each cave. Typical soil  
363 thicknesses are 0.5m for Soreq and 0.15m for Tzavoa, and carbonate rock  
364 thicknesses from surface to cave-level are  $\sim 30\text{m}$  for both. The rock is >98%  
365 carbonate by mass in Soreq and 97% carbonate at Tzavoa. With measured Li  
366 concentrations (Table 1), including those from the leaching experiments (which  
367 show that silicate-derived Li dominates the mass balance), this mass balance  
368 indicates that 70–78% of the total Li is in the soil silicate, 22–28% in rock  
369 silicate, and 1–2% in rock carbonate (Fig. 6). In actual fact, the amount of Li in  
370 the speleothems that derived from soil silicates is likely considerably higher, as  
371 the soils have a far greater proportion of high-activity (easily dissolvable)  
372 primary silicates than the carbonate rocks.

373         The relative dissolution rates of carbonates to silicates are harder to  
374 quantify, but a simple mass balance of Soreq's  $^{87}\text{Sr}/^{86}\text{Sr}$  data (Bar-Matthews et  
375 al., 1999; Palchan et al., 2013) suggest  $\sim 10\text{--}20\%$  of speleothem Sr comes from  
376 silicate dissolution, and that carbonates are dissolving  $\sim 6\times$  faster than silicates.  
377 Given that the ratio of Sr in silicates/carbonates is  $\sim 2000\times$  less than for Li, this  
378 suggests that >99.9% of Li in speleothems stems from silicate dissolution.

379         Overall, therefore, the speleothem Li dominantly stems from the  
380 weathering of the silicate portion of the overlying soils, which are largely aeolian,  
381 derived from the Northern Sinai and Nile Delta (mixed granitic-basaltic in origin)  
382 and from the Saharan-Arabian desert (granitic) (Ben-Israel et al., 2015; Ganor

383 and Foner, 2001; Palchan et al., 2013). Karst dissolution insignificantly affects  
384 the Li budgets of the drip waters and speleothems, because of the negligible  
385 amount of Li in the carbonate rocks.

386

#### 387 *5.4 Potential controls on weathering and Li isotopes*

388 The dominance of silicate weathering to the Li supply in these  
389 speleothems allows an assessment of the processes limiting silicate weathering  
390 in these areas and on these timescales. Parameters known to control silicate  
391 weathering rates (West et al., 2005), are i) changing supply of silicate, ii) soil or  
392 weathering zone thickness, iii) water supply, iv) vegetation and v) temperature.  
393 In this list, the weathering reactions of i) and ii) are limited by supply of silicate  
394 material, while those of iii), iv) and v) are controlled by the kinetics of the  
395 chemical reactions for each controlling process. These parameters are discussed  
396 generally here, and specifically for the studied caves in Section 5.5.

397

- 398 1) If the supply of primary silicates to the soil increases (e.g. changing dust  
399 supply rate), then the ratio of primary silicate dust dissolution to  
400 secondary mineral formation will increase. This will result in an increase  
401 in  $[\text{Li}]_{\text{diss}}$ , and a decrease in  $\delta^7\text{Li}_{\text{diss}}$  (where the subscript diss signifies the  
402 dissolved phase).
- 403 2) If the soil thickness (depth) increases, the overall thickness of weathering  
404 zone will increase and the water-rock interaction time also increases to  
405 allow greater secondary mineral formation, driving  $\delta^7\text{Li}_{\text{diss}}$  high.
- 406 3) If the water supply (i.e. rainfall) increases so that water flows through the  
407 soil more quickly, then the supply of undersaturated water increases.  
408 Higher water supply would therefore promote primary rock dissolution

409 relative to secondary mineral formation and decrease water-rock  
410 interaction time, both of which would drive  $\delta^{7}\text{Li}_{\text{diss}}$  towards lower, more  
411 rock-like, values.

412 4) It is more difficult to predict the effects of changing temperature on the  
413 congruency of weathering, because it is unknown precisely how  
414 temperature affects dissolution and the formation of secondary minerals,  
415 and the relative change of these two processes, even in weathering  
416 regimes such as here where material supply is not limiting the weathering  
417 reaction, and therefore kinetics dominate (West et al., 2005). Both natural  
418 and experimental studies have shown that dissolution rates of common  
419 silicate minerals increase 2–10% for every degree of temperature  
420 increase (once runoff effects are normalised (Eiriksdottir et al., 2013;  
421 Gislason et al., 2009)). Equally, the solubility of most (non-oxide)  
422 secondary minerals increases with temperature (Stefansson and Gislason,  
423 2001) so that their formation is less favoured as temperature increases.  
424 These two temperature dependencies suggest that higher temperatures  
425 promote primary mineral dissolution relative to secondary mineral  
426 formation. Riverine fluxes of other elements that are affected by  
427 secondary mineral formation, such as Ca or Mg, confirm this, with  
428 discharge-normalised fluxes increasing with temperature. This increase  
429 is less pronounced for Na, which is much less impacted by secondary  
430 mineral formation (Eiriksdottir et al., 2013; Gislason et al., 2009),  
431 suggesting that the temperature dependence is driven by both primary  
432 mineral dissolution and secondary mineral formation. Higher  
433 temperature is therefore expected to increase the congruency of  
434 weathering, leading to less removal of isotopically light Li into secondary

435 minerals (Pistiner and Henderson, 2003; Vigier et al., 2008; Wimpenny et  
436 al., 2015; Wimpenny et al., 2010), and therefore a lower  $\delta^7\text{Li}_{\text{diss}}$ .

437

438 In summary, thicker soil is expected to increase  $\delta^7\text{Li}_{\text{diss}}$ , while increased rainfall,  
439 silicate supply, or temperature should decrease it.

440

#### 441 *5.5 Determining the controls on Israeli $\delta^7\text{Li}$ and weathering*

442 The theoretical controls on  $\delta^7\text{Li}$  discussed in the previous section,  
443 combined with the well-understood field area of this study, allows us to  
444 determine the processes controlling changes in weathering conditions at this  
445 location during the last two glacial cycles. The process(es) controlling Li  
446 fractionation must explain the more incongruent weathering (i.e. higher  
447  $\delta^7\text{Li}_{\text{speleo}}$ ) experienced during glacial periods, and the general similarity of the  
448 two cave records relative to one another despite their different settings and  
449 secondary mineralogy in the modern (Sandler, 2013; Sandler et al., 2015), where  
450 it must also be stressed that variations in primary mineralogy in both settings is  
451 less important, as they have a very narrow range in  $\delta^7\text{Li}$ .

452 There is also a glacial-to-interglacial difference in [Li] in the two caves  
453 (Fig 4), though not as clear as that for  $\delta^7\text{Li}$ . The controls on trace-metal  
454 concentrations in speleothems have been extensively studied (e.g. Day and  
455 Henderson, 2013; Fairchild and Treble, 2009) and, although Li has not been  
456 amongst the trace elements typically measured, controls on speleothem Li/Ca  
457 can be assessed by analogy with other elements. For elements with a low  
458 partition coefficient into carbonate, including Li and frequently measured  
459 elements such as Mg, Sr and Ba, a dominant control is often the amount of calcite

460 precipitated from karst waters before they reach the speleothem growth surface  
461 (i.e. prior-calcite precipitation). This process would be expected to yield higher  
462 Li/Ca during dry periods, which is the opposite to that observed. For [Li] there is  
463 also an inverse dependence of partitioning into carbonate with temperature  
464 (Marriott et al., 2004). Glacial temperatures were  $\sim 10^{\circ}\text{C}$  colder than  
465 interglacials at Soreq (Affek et al., 2008) which would be expected to lead to  
466 Li/Ca  $\sim 2\times$  higher in the glacials, possibly explaining much of the change in Li/Ca.  
467 Weathering changes (e.g. dust supply) may also contribute to changes in Li/Ca  
468 with time, but will be only one of several processes influencing the ratio. This  
469 highlights the advantage of Li isotopes as a specific tracer for weathering. Prior-  
470 calcite-precipitation is not expected to generate large change in  $\delta^7\text{Li}$ , and there is  
471 no dependency of  $\delta^7\text{Li}$  with temperature (Marriott et al., 2004), so that  
472 weathering changes are expected to be the dominant control on  $\delta^7\text{Li}$ .

473

#### 474 5.5.1 Supply of silicate

475 The relatively short residence time ( $<10\text{--}14\text{ ka}$  – Section 2.3) of the  
476 present soils means it is theoretically possible that changing glacial-interglacial  
477 aeolian supply could control the observed  $\delta^7\text{Li}_{\text{speleo}}$  signals. However, an  
478 increased dust supply, which in Israel occurred during the glacials (Crouvi et al.,  
479 2009; Enzel et al., 2008), would decrease  $\delta^7\text{Li}_{\text{diss}}$  by providing fresh mineral  
480 surfaces. This is the opposite from the observed trend (Fig. 5), implying that the  
481 changes in weathering recorded by  $\delta^7\text{Li}_{\text{speleo}}$  variations are not limited by dust  
482 supply variations.

483 Further, at present and over the past three interglacials, Soreq has  
484 received smaller amounts of dust than Tzavoa, because of its greater distance

485 from the source (Crouvi et al., 2008; Enzel et al., 2008; Ganor and Foner, 2001).  
486 Soreq only received similar dust to Tzavoa during glacial periods when sea level  
487 decreased, and the northern coast of Sinai was located a few tens of km further  
488 to the north (Enzel et al., 2008) (Fig. 1b). The similarity in  $\delta^7\text{Li}_{\text{speleo}}$  between the  
489 two caves therefore argues against a regime in which weathering reactions are  
490 limited by supply of silicate dust.

491

### 492 5.5.2 Soil thickness

493 The thickness of the soil above the caves is primarily a function of the  
494 dust supply (see above) and removal by erosion and chemical weathering. There  
495 is little soil accumulation on the modern hill-slopes (except in isolated pockets),  
496 but more so on the flatter hill-tops (e.g. Fig. 2b). Soils were thought to be thicker  
497 in the last glacial than at present (Faershtein et al., 2016). Thicker soils would  
498 increase  $\delta^7\text{Li}_{\text{diss}}$ , meaning that higher  $\delta^7\text{Li}_{\text{speleo}}$  in the glacials (as observed) could  
499 suggest a soil thickness control on  $\delta^7\text{Li}_{\text{diss}}$  and silicate weathering. However, the  
500 timing of dust fluxes in the region does not agree with the observed  $\delta^7\text{Li}_{\text{speleo}}$   
501 patterns: dust fluxes started increasing at 95 ka, thickening soil cover during the  
502 glacials (Crouvi et al., 2008), while Soreq has approximately constant  $\delta^7\text{Li}_{\text{speleo}}$   
503 from ~128 to 68 ka (Fig. 5). In addition, the timing of loess buildup and loss in  
504 the Negev highlands during the last glacial period does not correspond to  
505 Tzavoa's  $\delta^7\text{Li}_{\text{speleo}}$  pattern. Soil thickness there increased from ~95 ka until 28 ka,  
506 after which loess supply decreased and erosion washed the soil into the valleys  
507 (Crouvi et al., 2008; Faershtein et al., 2016). By 24 ka, the colluvium was  
508 exposed, which was eroded along with the underlying sediment, with extensive  
509 incision occurring towards the end of that time period (Faershtein et al., 2016).

510 However, from ~33 to 14 ka,  $\delta^7\text{Li}_{\text{speleo}}$  values in Tzavoa are unchanged (Fig. 5).  
511 Hence, while the generally greater soil thickness during the glacials would drive  
512 solution  $\delta^7\text{Li}_{\text{diss}}$  higher (as observed), the detail in timing between evidence of  
513 soil thickness and  $\delta^7\text{Li}$  suggests that the former is not significantly controlling  
514 the latter. In MIS-5e, however, Tzavoa generally has lower  $\delta^7\text{Li}_{\text{speleo}}$  than Soreq by  
515 ~4‰. This might be explained by vegetative stabilisation of soil cover above  
516 Soreq Cave, leading to thicker soils than those above Tzavoa (see 5.5.4) during  
517 this period only.

518

### 519 5.5.3 Rainfall

520 Influx from rainfall was higher at both caves during glacials (Ayalon et al.,  
521 1999; Vaks et al., 2006), which is expected to lower  $\delta^7\text{Li}_{\text{diss}}$ , the opposite from  
522 that observed. Further, Soreq cave was always wetter than Tzavoa, because of  
523 Tzavoa's remoteness from the Mediterranean storm tracks (Vaks et al., 2006),  
524 but the two caves have similar  $\delta^7\text{Li}_{\text{speleo}}$  values (Fig. 5). This suggests that water  
525 supply was not limiting silicate weathering.

526

### 527 5.5.4 Vegetation

528 The same argument also applies to vegetation. Soreq is more vegetated  
529 than Tzavoa, but the similar  $\delta^7\text{Li}_{\text{speleo}}$  behaviour implies that vegetation is not  
530 limiting weathering. In MIS-5e, however, Tzavoa generally has lower  $\delta^7\text{Li}_{\text{speleo}}$   
531 than Soreq by ~4‰. Vegetative stabilisation of soil thickness may play a role  
532 here, as Soreq has thicker, more stable, soils.

533

### 534 5.5.5 Temperature

535           The final potential control on Li isotopes and weathering in these regions  
536 is temperature. Lower temperatures during glacials could explain the higher  
537  $\delta^7\text{Li}_{\text{speleo}}$  values observed at both caves during these periods, and the similar  
538 temperatures at the two caves can explain the similar  $\delta^7\text{Li}_{\text{speleo}}$  between them.  
539 Palaeo-temperatures have been determined from Soreq and the marine record  
540 from three separate studies, using clumped isotopes (Affek et al., 2008) and fluid  
541 inclusions from Soreq (McGarry et al., 2004) and alkenones from a nearby  
542 marine core (Almogi-Labin et al., 2009). There is a strong correlation between  
543 temperature and speleothem  $\delta^7\text{Li}$ , with lower  $\delta^7\text{Li}_{\text{speleo}}$  values at higher  
544 temperatures (Fig. 7), further supporting the importance of temperature in  
545 controlling the observed  $\delta^7\text{Li}$  change. This variability cannot be caused by a  
546 temperature-controlled change in the fractionation of Li isotopes during growth  
547 of secondary minerals, because the temperature dependence of this fractionation  
548 is small (Vigier et al., 2008) and, with the observed temperature change, would  
549 only cause a 0.1–1.7‰ change in fractionation. Instead, this implies that silicate  
550 weathering is more congruent when temperatures are higher, due to a  
551 temperature-control on both primary and secondary mineral solubility, as  
552 discussed in Section 5.4.

553

#### 554 *5.6 Implications for silicate weathering*

555           For a given isotopic fractionation factor during secondary mineral  
556 formation, the fraction of Li in solution relative to that incorporated into  
557 secondary minerals ( $f_w$ ) can be calculated using the formula (Pogge von  
558 Strandmann et al., 2012):

559

560  $d_w = d_w^i + 1000(a - 1) \times \ln(f_w)$

561

562 where  $\delta_w$  is the  $\delta^7\text{Li}$  of water (i.e. corrected for uptake into calcite), and  $\delta_w^i$  is the  
563 starting composition (i.e. the  $\delta^7\text{Li}$  of the host soils). In this case, we use the  
564 fractionation factor  $\alpha = 0.98$ , which is the difference between modern drip  
565 waters and silicate fractions of the overlying soils. Notably, using this  
566 fractionation factor requires a Rayleigh relationship, as equilibrium could not  
567 cause the observed amount of fractionation for this fractionation factor. This  
568 shows that the amount of Li in solution was on average 25% greater during  
569 interglacials than glacials, and was almost twice as great shortly after  
570 deglaciation, compared to glacial maxima (Fig. 8).

571         The implication is that the silicate weathering congruency or efficiency  
572 (lithium released per unit of silicate rock (Pogge von Strandmann et al., 2016;  
573 Pogge von Strandmann and Henderson, 2015)) was higher during interglacials.  
574 This can also be extrapolated to the cations that play a significant role in the  
575 carbon cycle, calcium and magnesium. Both are affected by secondary mineral  
576 formation and sorption similarly to Li, and, in basaltic weathering regimes where  
577 quantification is relatively straightforward, are as mobile as Li within a factor of  
578 2–4 (Pogge von Strandmann et al., 2016). In contrast, quantifying these  
579 mobilities during granite weathering is not yet possible, given a lack of data.  
580 Hence, in these soils that are mixtures of basaltic and granitic dust, Li isotopes  
581 provide a qualitative measure of the efficiency of  $\text{CO}_2$  sequestration, but further  
582 work is required before they can be quantitatively related to the trapping of Ca  
583 and Mg in continental clays.

584 Overall, therefore, because more congruent weathering ultimately results  
585 in less cations sequestered into secondary minerals, the data imply that CO<sub>2</sub>  
586 drawdown efficiency (unit CO<sub>2</sub> sequestered per unit silicate rock) in these semi-  
587 arid areas of Israel was greater in interglacials. While it is difficult to calculate  
588 weathering rates directly from Li isotopes (Pogge von Strandmann et al., 2017),  
589 weathering processes in this area appear to be responding to a climatic control.  
590 Determining the effect on global seawater is difficult, because different signals  
591 may counteract each other, creating less variability in seawater (Foster and  
592 Vance, 2006; von Blanckenburg et al., 2015). Hence, seawater and its archives  
593 may be less useful in examining weathering over relatively short timescales than  
594 continental records such as speleothems.

595

## 596 6.0 Conclusions

597 This study has analysed Li isotope ratios from speleothems, which formed  
598 during the last 200kyr in two Israeli caves distinct in their modern climates,  
599 Soreq and Tzavoa, as well as accompanying rocks, soils and drip waters. The goal  
600 was to test the use of speleothems as an archive to capture the silicate  
601 weathering proxy,  $\delta^7\text{Li}$ , and to assess local controls on silicate weathering in a  
602 continental archive, rather than using marine records which average over broad  
603 geographical regions (or globally). Such local records are critical in assessing the  
604 processes that control weathering, and hence how weathering alters with  
605 climate change.

606 Host-rock and soils analysis shows that Li stems from weathering of soils  
607 composed of aeolian silicates. The speleothem Li isotopes show a ubiquitous  
608 trend of lower  $\delta^7\text{Li}_{\text{speleo}}$  values during interglacials, with the most rapid decrease  
609 immediately after the two sampled deglaciations. The pattern of change and

610 absolute  $\delta^7\text{Li}_{\text{speleo}}$  values are very similar in the two caves. The  $\delta^7\text{Li}$  changes  
611 cannot readily be explained by changes in dust supply or soil thickness (except  
612 possibly during interglacial MIS-5.5). Instead,  $\delta^7\text{Li}_{\text{speleo}}$  variations are explained  
613 by temperature change, with which they correlate well. Lower  $\delta^7\text{Li}_{\text{speleo}}$   
614 correlates with higher temperatures of the interglacials. This suggests that  
615 primary rock dissolution is enhanced relative to secondary mineral formation as  
616 temperatures increase, in agreement with modern weathering studies. The data  
617 indicate the potential for use of  $\delta^7\text{Li}$  analysis in speleothems to assess past  
618 weathering, and show that, for this Israeli semi-arid region, silicate weathering  
619 becomes more congruent at higher temperatures.

620

#### 621 Acknowledgements

622 Yuval Burstyn is thanked for collecting drip waters, soils and recent carbonates.  
623 The Israel Nature and Parks Authority is thanked for sampling permits. Phil  
624 Holdship is thanked for assistance with concentration analyses. Analyses and  
625 PPvS were funded by NERC advanced fellowship NE/I020571/2 and ERC  
626 Consolidator grant 682760 - CONTROLPASTCO2, while some additional analyses  
627 were funded by NERC fellowship NE/G013829/1. This manuscript was  
628 improved by reviews from Friedhelm von Blanckenburg and two anonymous  
629 reviewers.

630

631

#### 632 References

633

634 Affek, H.P., Bar-Matthews, M., Ayalon, A., Matthews, A., Eiler, J.M., 2008.  
635 Glacial/interglacial temperature variations in Soreq cave speleothems as

636 recorded by 'clumped isotope' thermometry. *Geochim. Cosmochim. Acta* 72,  
637 5351–5360.

638 Almogi-Labin, A., Bar-Matthews, M., Shriki, D., Kolosovsky, E., Paterne, M.,  
639 Schilman, B., Ayalon, A., Aizenshtat, Z., Matthews, A., 2009. Climatic variability  
640 during the last ~90 ka of the southern and northern Levantine Basin as evident  
641 from marine records and speleothems. *Quaternary Science Reviews* 28, 2882-  
642 2896.

643 Amit, R., Enzel, Y., Crouvi, O., Simhai, O., Matmon, A., Porat, N., McDonald, E.,  
644 Gillespie, A.R., 2011. The role of the Nile in initiating a massive dust influx to the  
645 Negev late in the middle Pleistocene. *Geol. Soc. Am. Bull.* 123, 873-889.

646 Archer, D., Winguth, A., Lea, D.W., Mahowald, N., 2000. What causes the  
647 glacial/interglacial atmospheric pCO<sub>2</sub> cycles? *Rev. Geophys.* 38, 159-189.

648 Ayalon, A., Bar-Matthews, M., Kaufman, A.J., 1999. Petrography, strontium,  
649 barium and uranium concentrations, and strontium and uranium isotope ratios  
650 in speleothems as palaeoclimatic proxies: Soreq Cave, Israel. *The Holocene* 9,  
651 715–722.

652 Bar-Matthews, M., Ayalon, A., Gilmour, M., Matthews, A., Hawkesworth, C.J., 2003.  
653 Sea-land oxygen isotopic relationships from planktonic foraminifera and  
654 speleothems in the Eastern Mediterranean region and their implication for  
655 paleorainfall during interglacial intervals. *Geochim. Cosmochim. Acta* 67, 3181-  
656 3199.

657 Bar-Matthews, M., Ayalon, A., Kaufman, A.J., Wasserburg, G.J., 1999. The Eastern  
658 Mediterranean paleoclimate as a reflection of regional events: Soreq cave, Israel.  
659 *Earth Planet. Sci. Lett.* 166, 85–95.

660 Ben-Israel, M., Enzel, Y., Amit, R., Erel, Y., 2015. Provenance of the various grain-  
661 size fractions in the Negev loess and potential changes in major dust sources to  
662 the Eastern Mediterranean. *Quaternary Research* 83, 105–115.

663 Burton, K.W., Vance, D., 2000. Glacial-interglacial variations in the neodymium  
664 isotope composition of seawater in the Bay of Bengal recorded by planktonic  
665 foraminifera. *Earth Planet. Sci. Lett.* 176, 425-441.

666 Clergue, C., Dellinger, M., Buss, H.L., Gaillardet, J., Benedetti, M.F., Dessert, C.,  
667 2015. Influence of atmospheric deposits and secondary minerals on Li isotopes  
668 budget in a highly weathered catchment, Guadeloupe (Lesser Antilles). *Chem.*  
669 *Geol.* 414, 28–41.

670 Coge, A., Meynadier, L., Allegre, C.J., Limmois, D., Herman, F., Gaillardet, J., 2015.  
671 Constraints on the role of tectonic and climate on erosion revealed by two time  
672 series analysis of marine cores around New Zealand. *Earth Planet. Sci. Lett.* 410,  
673 174–185.

674 Crocket, K.C., Foster, G.L., Vance, D., Richards, D.A., Tranter, M., 2013. A Pb  
675 isotope tracer of ocean-ice sheet interaction: the record from the NE Atlantic  
676 during the Last Glacial/Interglacial cycle. *Quaternary Science Reviews* 82, 133-  
677 144.

678 Crouvi, O., Amit, R., Enzel, Y., Gillespie, A.R., 2010. Active sand seas and the  
679 formation of desert loess. *Quaternary Science Reviews* 29, 2087-2098.

680 Crouvi, O., Amit, R., Enzel, Y., Porat, N., McDonald, E.V., 2007. Regional  
681 pedosedimentary stratigraphic units in the primary eolian loess of the Negev  
682 Desert, Israel, in: Crouvi, O., Malik, U., Oren, O., Shalev, E., Friedman, V., Yechieli,  
683 Y. (Eds.), *Israel Geological Society, Annual Meeting: Neven Zohar, The Dead Sea.*

684 Crouvi, O., Amit, R., Enzel, Y., Porat, N., Sandler, A., 2008. Sand dunes as a major  
685 proximal dust source for late Pleistocene loess in the Negev desert, Israel.  
686 *Quaternary Research* 70, 275–282.

687 Crouvi, O., Amit, R., Porat, N., Gillespie, A.R., McDonald, E.V., Enzel, Y., 2009.  
688 Significance of primary hilltop loess in reconstructing dust chronology, accretion  
689 rates, and sources: An example from the Negev Desert, Israel. *Journal of*  
690 *Geophysical Research* 114, F0217.

691 Day, C.C., Henderson, G.M., 2013. Controls on Trace-element Partitioning in Cave-  
692 analogue Calcite. *Geochim. Cosmochim. Acta* 120, 612–627.

693 Dellinger, M., Gaillardet, J., Bouchez, J., Calmels, D., Louvat, P., Dosseto, A., Gorge,  
694 C., Alanoca, L., Maurice, L., 2015. Riverine Li isotope fractionation in the Amazon  
695 River basin controlled by the weathering regimes. *Geochim. Cosmochim. Acta*  
696 164, 71–93.

697 Eiriksdottir, E.S., Gislason, S.R., Oelkers, E.H., 2013. Does temperature or runoff  
698 control the feedback between chemical denudation and climate? Insights from  
699 NE Iceland. *Geochim. Cosmochim. Acta* 107, 65–81.

700 Enzel, Y., Amit, R., Dayan, U., Crouvi, O., Kahana, R., Ziv, B., Sharon, D., 2008. The  
701 climatic and physiographic controls of the eastern Mediterranean over the late  
702 Pleistocene climates in the southern Levant and its neighboring deserts. *Glob.*  
703 *Planet. Change* 60, 165-192.

704 Faershtein, G., Porat, N., Avni, Y., Matmon, A., 2016. Aggradation–incision  
705 transition in arid environments at the end of the Pleistocene: An example from  
706 the Negev Highlands, southern Israel. *Geomorphology* 253, 289-304.

707 Fairchild, I.J., Treble, P.C., 2009. Trace Elements in Speleothems As Recorders of  
708 Environmental Change. *Quaternary Science Reviews* 28.

709 Foster, G.L., Vance, D., 2006. Negligible glacial-interglacial variation in  
710 continental chemical weathering rates. *Nature* 444, 918-921.

711 Frings, P.J., Clymans, W., Fontorbe, G., De la Rocha, C.L., Conley, D.J., 2016. The  
712 continental Si cycle and its impact on the ocean Si isotope budget. *Chem. Geol.*  
713 425, 12–36.

714 Frumkin, A., Fischhendler, I., 2005. Morphometry and distribution of isolated  
715 caves as a guide for phreatic and confined paleohydrological conditions.  
716 *Geomorphology* 67, 457-471.

717 Frumkin, A., Stein, M., 2004. The Sahara-East Mediterranean dust and climate  
718 connection revealed by strontium and uranium isotopes in a Jerusalem  
719 speleothem. *Earth Planet. Sci. Lett.* 217, 451-464.

720 Gadot, Y., Davidovich, U., Avni, G., Avni, Y., Piasezky, M., Faershtein, G., Golan, D.,  
721 Porat, N., 2016. The formation of a Mediterranean terraced landscape: Mount  
722 Eitan, Judean Highlands, Israel. *Journal of Archaeological Science: Reports* 6, 397-  
723 417.

724 Ganor, E., Foner, H.A., 2001. Mineral dust concentrations, deposition fluxes and  
725 deposition velocities in dust episodes over Israel. *Journal of Geophysical*  
726 *Research* 106, 18431-18437.

727 Gislason, S.R., Oelkers, E.H., Eiriksdottir, E.S., Kardjilov, M.I., Gisladottir, G.,  
728 Sigfusson, B., Snorrason, A., Elefsen, S., Hardardottir, J., Torssander, P., Oskarsson,  
729 N., 2009. Direct evidence of the feedback between climate and weathering. *Earth*  
730 *Planet. Sci. Lett.* 277, 213-222.

731 Gurlan, A.T., Meynadier, L., Allegre, C.J., Tapponnier, P., Birck, J.L., Joron, J.-L.,  
732 2010. Northern Hemisphere climate control of the Bengali rivers discharge  
733 during the past 4 Ma. *Quaternary Science Reviews* 29, 2484–2498.

734 Grant, K.M., Rohling, E.J., Bar-Matthews, M., Ayalon, A., Medina-Elizalde, M.,  
735 Ramsey, C.B., Satow, C., Roberts, A.P., 2012. Rapid coupling between ice volume  
736 and polar temperature over the past 150,000 years. *Nature* 491, 744-747.

737 Hathorne, E.C., James, R.H., 2006. Temporal record of lithium in seawater: a  
738 tracer for silicate weathering? *Earth Planet. Sci. Lett.* 246, 393–406.

739 Huh, Y., Chan, L.H., Zhang, L., Edmond, J.M., 1998. Lithium and its isotopes in  
740 major world rivers: Implications for weathering and the oceanic budget.  
741 *Geochim. Cosmochim. Acta* 62, 2039–2051.

742 Kiskurek, B., James, R.H., Harris, N.B.W., 2005. Li and  $\delta^7\text{Li}$  in Himalayan rivers:  
743 Proxies for silicate weathering? *Earth Planet. Sci. Lett.* 237, 387–401.

744 Le Roux, P.J., 2010. Lithium isotope analysis of natural and synthetic glass by  
745 laser ablation MC-ICP-MS. *J. Anal. At. Spectrom.* 25, 1033–1038.

746 Lechler, M., Pogge von Strandmann, P.A.E., Jenkyns, H.C., Prosser, G., Parente, M.,  
747 2015. Lithium-isotope evidence for enhanced silicate weathering during OAE 1a  
748 (Early Aptian Selli event). *Earth Planet. Sci. Lett.* 432, 210–222.

749 Ludwig, W., Amiotte-Suchet, P., Probst, J.-L., 1999. Enhanced chemical  
750 weathering of rocks during the last glacial maximum: a sink for atmospheric  
751 CO<sub>2</sub>? *Chem. Geol.* 159, 147–161.

752 Mamane, Y., 1987. Chemistry of precipitation in Israel. *Sci. Total Environ.* 61, 1–  
753 13.

754 Mamane, Y., Dayan, U., Miller, J.M., 1987. Contribution of alkaline and acidic  
755 sources to precipitation in Israel. *Sci. Total Environ.* 61, 15–22.

756 Marriott, C.S., Henderson, G.M., Crompton, R., Staubwasser, M., Shaw, S., 2004.  
757 Effect of mineralogy, salinity, and temperature on Li/Ca and Li isotope  
758 composition of calcium carbonate. *Chem. Geol.* 212, 5–15.

759 McGarry, S., Bar-Matthews, M., Matthews, A., Vaks, A., Schilman, B., Ayalon, A.,  
760 2004. Constraints on hydrological and paleotemperature variations in the  
761 Eastern Mediterranean region in the last 140 ka given by the  $\delta\text{D}$  values of  
762 speleothem fluid inclusions. *Quaternary Science Reviews* 23, 919–934.

763 Mokadem, F., Parkinson, I.J., Hathorne, E.C., Anand, P., Allen, J.T., Burton, K.W.,  
764 2015. High-precision radiogenic strontium isotope measurements of the modern  
765 and glacial ocean: Limits on glacial–interglacial variations in continental  
766 weathering. *Earth Planet. Sci. Lett.* 415, 111–120.

767 Munhoven, G., 2002. Glacial-interglacial changes of continental weathering:  
768 estimates of the related CO<sub>2</sub> and HCO<sub>3</sub><sup>-</sup> flux variations and their uncertainties.  
769 *Glob. Planet. Change* 33, 155–176.

770 Munhoven, G., Francois, L.M., 1996. Glacial-interglacial variability of atmospheric  
771 CO<sub>2</sub> due to changing continental silicate rock weathering: A model study. *J.*  
772 *Geophys. Res.-Atmos.* 101, 21423–21437.

773 Orland, I.J., Burstyn, Y., Bar-Matthews, M., Kozdon, R., Ayalon, A., Matthews, A.,  
774 Valley, J.W., 2014. Seasonal climate signals (1990–2008) in a modern Soreq Cave  
775 stalagmite as revealed by high-resolution geochemical analysis. *Chem. Geol.* 363,  
776 322–333.

777 Palchan, D., Stein, M., Almogi-Labin, A., Erel, Y., Goldstein, S.L., 2013. Dust  
778 transport and synoptic conditions over the Sahara–Arabia deserts during the  
779 MIS6/5 and 2/1 transitions from grain-size, chemical and isotopic properties of  
780 Red Sea cores. *Earth Planet. Sci. Lett.* 382, 125–139.

781 Phan, T.T., Capo, R.C., Stewart, B.W., Macpherson, G.L., Rowan, E.L., Hammack,  
782 R.W., 2016. Factors controlling Li concentration and isotopic composition in  
783 formation waters and host rocks of Marcellus Shale, Appalachian Basin. *Chem.*  
784 *Geol.* 420, 162–179.

785 Pistiner, J.S., Henderson, G.M., 2003. Lithium-isotope fractionation during  
786 continental weathering processes. *Earth Planet. Sci. Lett.* 214, 327–339.

787 Pogge von Strandmann, P.A.E., Burton, K.W., Opfergelt, S., Eiriksdottir, E.S.,  
788 Murphy, M.J., Einarsson, A., Gislason, S.R., 2016. The effect of hydrothermal  
789 spring weathering processes and primary productivity on lithium isotopes: Lake  
790 Myvatn, Iceland. *Chem. Geol.* in press.

791 Pogge von Strandmann, P.A.E., Frings, P.J., Murphy, M.J., 2017. Lithium isotope  
792 behaviour during weathering in the Ganges Alluvial Plain. *Geochim. Cosmochim.*  
793 *Acta* 198, 17–31.

794 Pogge von Strandmann, P.A.E., Henderson, G.M., 2015. The Li isotope response to  
795 mountain uplift. *Geology* 43, 67–70.

796 Pogge von Strandmann, P.A.E., Jenkyns, H.C., Woodfine, R.G., 2013. Lithium  
797 isotope evidence for enhanced weathering during Oceanic Anoxic Event 2.  
798 *Nature Geoscience* 6, 668–672.

799 Pogge von Strandmann, P.A.E., Opfergelt, S., Lai, Y.J., Sigfusson, B., Gislason, S.R.,  
800 Burton, K.W., 2012. Lithium, magnesium and silicon isotope behaviour  
801 accompanying weathering in a basaltic soil and pore water profile in Iceland.  
802 *Earth Planet. Sci. Lett.* 339–340, 11–23.

803 Sandler, A., 2013. Clay distribution over the landscape of Israel: From the hyper-  
804 arid to the Mediterranean climate regimes. *Catena* 110, 119–132.

805 Sandler, A., Meunier, A., Velde, B., 2015. Mineralogical and chemical variability of  
806 mountain red/brown Mediterranean soils. *Geoderma* 239–240, 156–167.

807 Stefansson, A., Gislason, S.R., 2001. Chemical weathering of basalts, Southwest  
808 Iceland: Effect of rock crystallinity and secondary minerals on chemical fluxes to  
809 the ocean. *Am. J. Sci.* 301, 513–556.

810 Teng, F.Z., McDonough, W.F., Rudnick, R.L., Dalpe, C., Tomascak, P.B., Chappell,  
811 B.W., Gao, S., 2004. Lithium isotopic composition and concentration of the upper  
812 continental crust. *Geochim. Cosmochim. Acta* 68, 4167–4178.

813 Vaks, A., Bar-Matthews, M., Ayalon, A., Matthews, A., Frumkin, A., Dayan, U.,  
814 Halicz, L., Almogi-Labin, A., Schilman, B., 2006. Paleoclimate and location of the  
815 border between Mediterranean climate region and the Saharo-Arabian Desert as  
816 revealed by speleothems from the northern Negev Desert, Israel *Earth Planet.*  
817 *Sci. Lett.* 249, 384–399.

818 Vaks, A., Gutareva, O.S., Breitenbach, S.F.M., Avirmed, E., Mason, A.J., Thomas, A.L.,  
819 Osinzev, A.V., Kononov, A.M., Henderson, G.M., 2013a. Speleothems Reveal  
820 500,000-Year History of Siberian Permafrost. *Science* 340 183–186.

821 Vaks, A., Woodhead, J., Bar-Matthews, M., Ayalon, A., Cliff, R.A., Zilberman, T.,  
822 Matthews, A., Frumkin, A., 2013b. Pliocene–Pleistocene climate of the northern  
823 margin of Saharan–Arabian Desert recorded in speleothems from the Negev  
824 Desert, Israel. *Earth Planet. Sci. Lett.* 368, 88–100.

825 Vance, D., Teagle, D.A.H., Foster, G.L., 2009. Variable Quaternary chemical  
826 weathering fluxes and imbalances in marine geochemical budgets. *Nature* 458,  
827 493–496.

828 Vigier, N., Decarreau, A., Millot, R., Carignan, J., Petit, S., France-Lanord, C., 2008.  
829 Quantifying Li isotope fractionation during smectite formation and implications  
830 for the Li cycle. *Geochim. Cosmochim. Acta* 72, 780–792.

831 von Blanckenburg, F., Bouchez, J., Ibarra, D.E., Maher, K., 2015. Stable runoff and  
832 weathering fluxes into the oceans over Quaternary climate cycles. *Nature*  
833 *Geoscience* 8, 538–542.

834 Wan, S., Clift, P.D., Zhao, D., Hovius, N., Munhoven, G., France-Lanord, C., Wang, Y.,  
835 Xiong, Z., Huang, J., Yu, Z., Zhang, J., Ma, W., G., Z., Li, A., Li, T., 2017. Enhanced  
836 silicate weathering of tropical shelf sediments exposed during glacial lowstands:  
837 A sink for atmospheric CO<sub>2</sub>. *Geochim. Cosmochim. Acta* 200, 123–144.

838 West, A.J., Galy, A., Bickle, M., 2005. Tectonic and climatic controls on silicate  
839 weathering. *Earth Planet. Sci. Lett.* 235, 211–228.  
840 Wilson, D.J., Galy, A., Piotrowski, A.M., Banakar, V.K., 2015. Quaternary climate  
841 modulation of Pb isotopes in the deep Indian Ocean linked to the Himalayan  
842 chemical weathering. *Earth Planet. Sci. Lett.* 424, 256–268.  
843 Wimpenny, J., Colla, C.A., Yu, P., Yin, Q.Z., Rustad, J.R., Casey, W.H., 2015. Lithium  
844 isotope fractionation during uptake by gibbsite. *Geochim. Cosmochim. Acta* 168,  
845 133–150.  
846 Wimpenny, J., Gislason, S.R., James, R.H., Gannoun, A., Pogge von Strandmann,  
847 P.A.E., Burton, K.W., 2010. The behaviour of Li and Mg isotopes during primary  
848 phase dissolution and secondary mineral formation in basalt. *Geochim.*  
849 *Cosmochim. Acta* 74, 5259–5279.  
850 Yaalon, D.H., 1997. Soils in the Mediterranean region: what makes them  
851 different? *Catena* 28, 157–169.  
852 Zeebe, R.E., Caldeira, K., 2008. Close mass balance of long-term carbon fluxes  
853 from ice-core CO<sub>2</sub> and ocean chemistry records. *Nature Geoscience* 1, 312–315.  
854

855

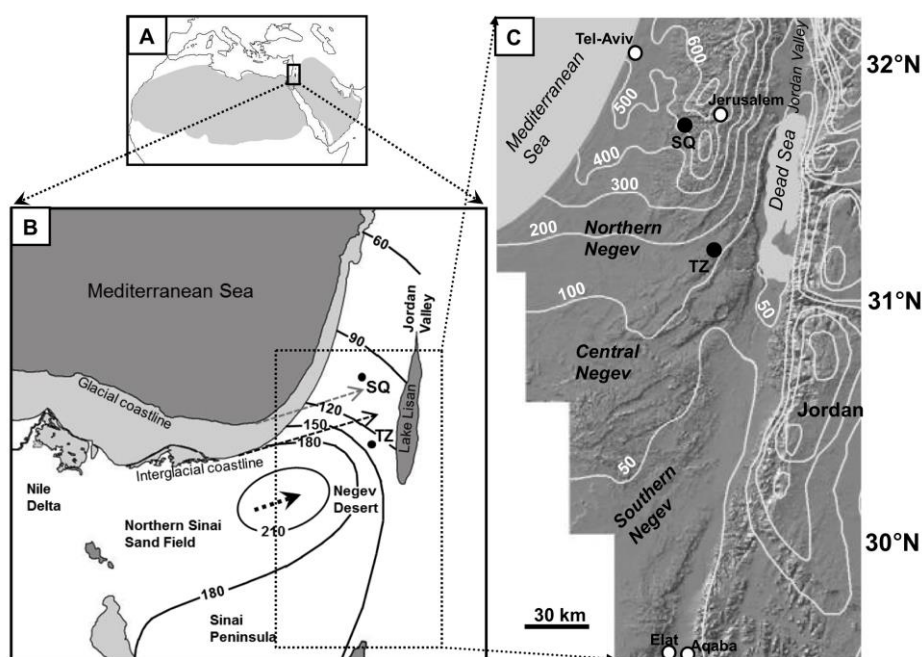
	$\delta^7\text{Li}$	2sd	Li ( $\mu\text{g/g}$ )	fLi (by total rock mass)
<b>Soreq</b>				
<i>Rock</i>				
Carbonate	22.3	0.5	0.05	0.05
Residue	10.2	0.1	49.7	0.95
Bulk rock	9.4	0.3	46.3	
<i>Soil</i>				
Exchangeable	13.5	0.3	0.01	0.0004
Carbonate	15.7	0.5	0.01	0.0004
Residue	1.6	0.2	31.7	0.9993
Bulk	1.6	0.4	32.0	
<b>Tzavoa</b>				
<i>Rock</i>				
Carbonate	20.1	0.2	0.06	0.04
Residue	6.1	0.4	42.5	0.96
Bulk rock	7.4	0.4	38.2	
<i>Soil</i>				
Exchangeable	11.9	0.2	0.01	0.0004
Carbonate	13.4	0.4	0.03	0.0013
Residue	2.5	0.8	22.5	0.9983
Bulk	3.2	0.2	22.9	

856

857

858 Table 1. Data from sequential extraction of the overlying soils and rocks. The  
 859 fraction of Li by total rock mass (fLi) was calculated from the mass of original  
 860 material lost during the leaching steps, and the measured Li abundance in the  
 861 individual phases (see text for details).  
 862  
 863

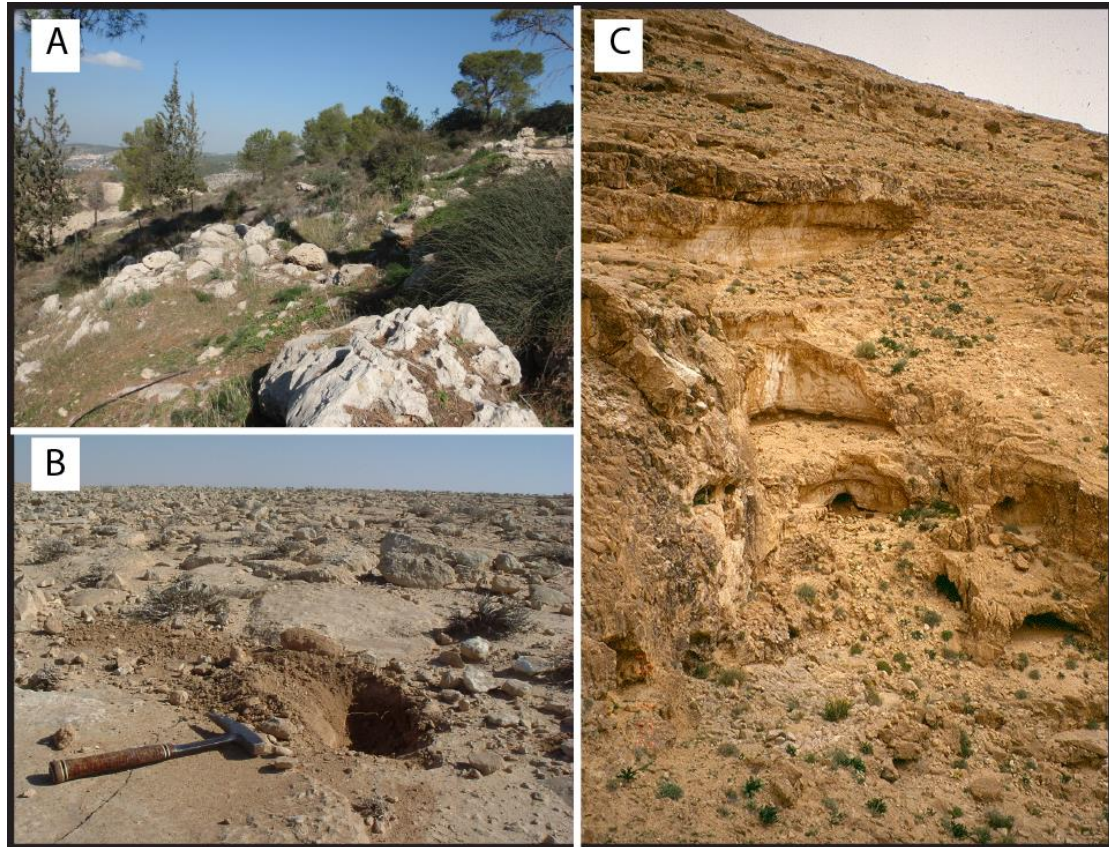
Figure 1



864  
 865 Figure 1. (A) Geographical position of the research area. Saharan-Arabian Desert  
 866 is shown in grey; (B) Glacial and interglacial positions of Sinai and Nile Delta  
 867 coast (Enzel et al., 2008), and the expected northward shift in location of the dust  
 868 plume. The present day dustfall map ( $\text{g}/\text{m}^2$  per year)(Ganor and Foner, 2001) is  
 869 shown by black contours, whereas the two studied caves, Tzavoa (TZ) and Soreq  
 870 (SQ) are shown as well. Thick and short arrow shows the W-S-W direction of  
 871 strong winds, blowing in the area during the passage of winter storms (Atlantic-  
 872 Mediterranean cyclones). Two thin arrows show how the dustfall contours may

873 shift northward with the shift of the coastline from interglacial (black arrow) to  
874 glacial position (grey arrow), with the same wind intensity. Lake Lisan shown on  
875 the map is a Last Glacial precursor of the Dead Sea; (C) Precipitation map of the  
876 research area with the locations of the two caves (Vaks et al., 2006).

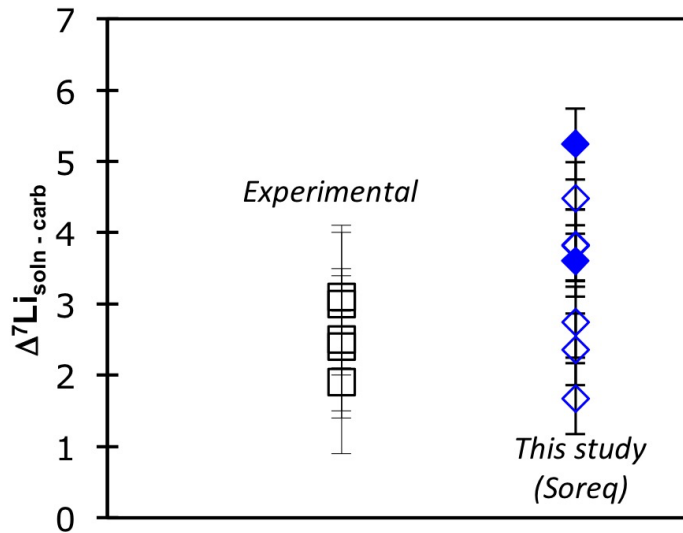
877



878

879 Figure 2. A) topography and vegetation above Soreq Cave; B) sampling of a soil  
880 pocket above Tzavoa Cave; C) topography and vegetation at the entrance of  
881 Tzavoa Cave (Photo by A. Frumkin).

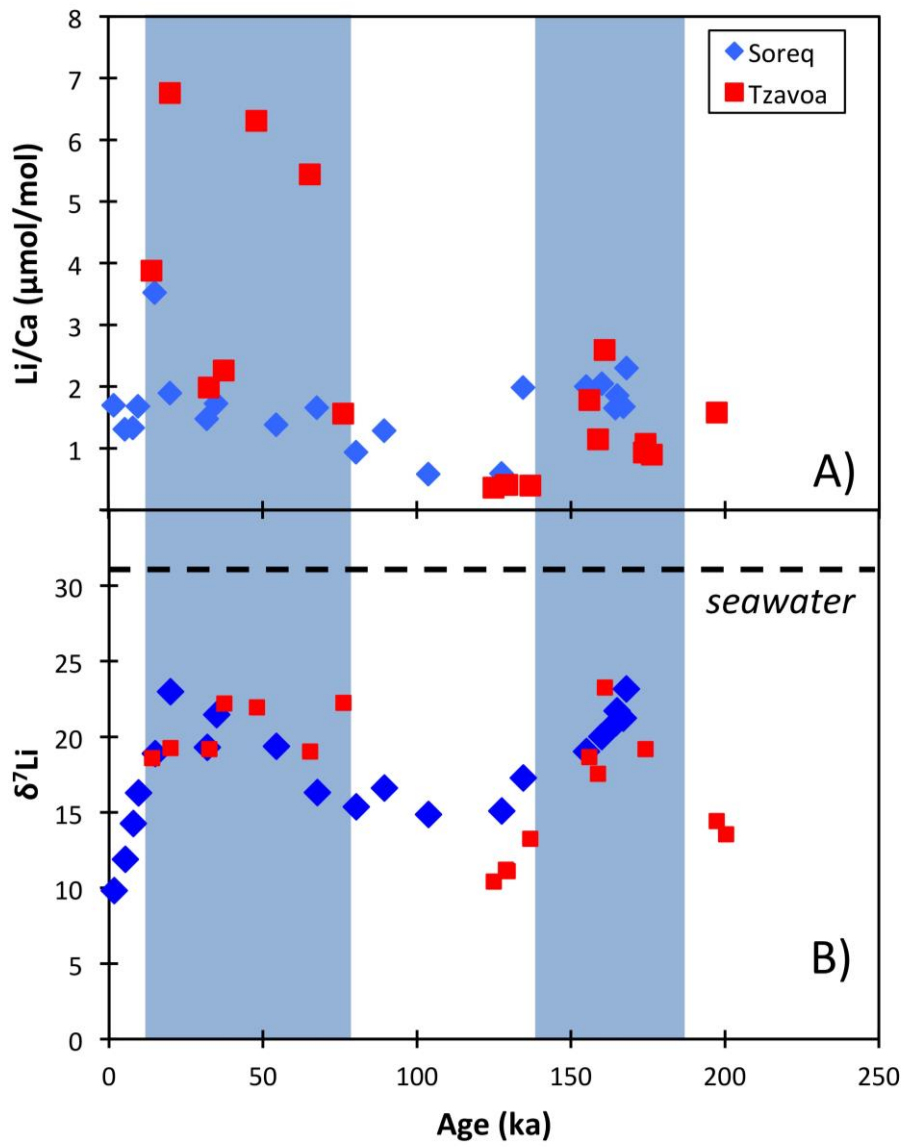
882



883

884 Figure 3. The Li isotopic difference between carbonate and solution for modern  
 885 drip waters and carbonates (this study) and experimental carbonates (Marriott  
 886 et al., 2004). For this study's carbonates (from Soreq), the closed symbols  
 887 represent samples of corresponding drip water and carbonates, while open  
 888 symbols represent drip waters sampled elsewhere in the cave, but only  
 889 compared to the same carbonates as above.

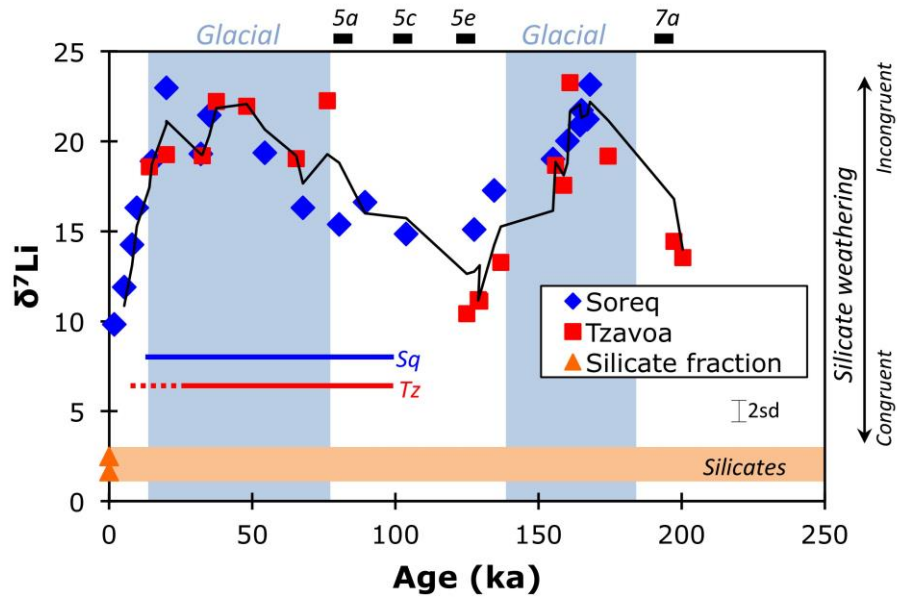
890



891

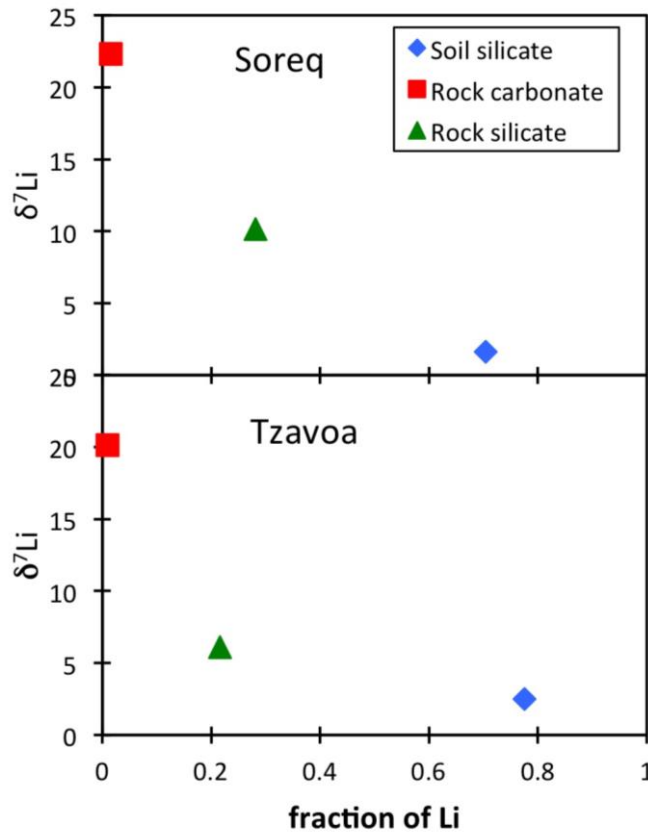
892 Figure 4. A) Li/Ca ratios of the speleothems compared to Li isotope ratios (B).

893



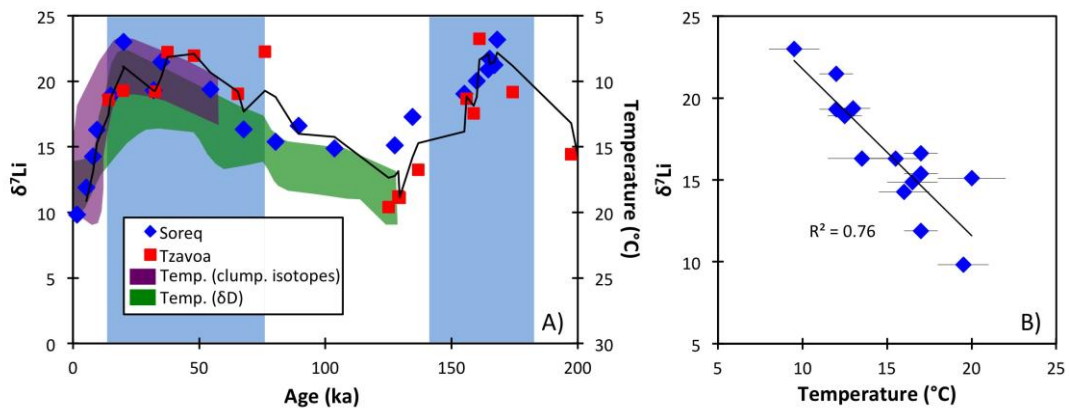
894

895 Figure 5: Lithium isotope data from speleothems in Soreq and Tzavoa caves,  
 896 where the black line represents a 2-point running average. Also shown are the  
 897 silicate soil  $\delta^7\text{Li}$  values from both cave sites. The solid horizontal blue and red  
 898 lines represent periods when soil was deposited at Soreq (Sq) (Crouvi et al.,  
 899 2009) and Tzavoa (Tz) (Faershtein et al., 2016). The dotted horizontal red line  
 900 represents periods when soil at Tzavoa was eroded and valleys incised  
 901 (Faershtein et al., 2016). The lack of correlation between this and  $\delta^7\text{Li}$  imply that  
 902 silicate supply is not controlling weathering. The black bars at the top of the  
 903 diagram represent MIS stages.



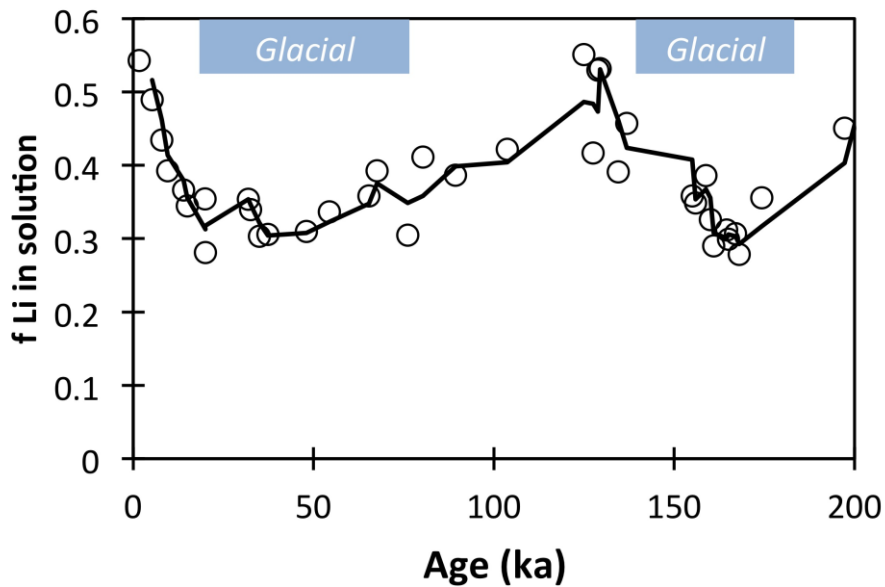
904

905 Figure 6. Li isotope composition plotted against the fraction of Li in each phase  
 906 from the entire cumulative thickness of rock or soil above each cave. The soil  
 907 silicate is likely an underestimate for Li available from the soil silicate fraction,  
 908 because the soils contain a large proportion of high-activity primary silicates that  
 909 dissolve more readily.



910

911 Figure 7. A) Li isotope ratios of speleothems plotted against time. Superimposed  
912 on the Li profile are palaeotemperatures from Soreq: the purple area represents  
913 temperatures data from clumped isotopes (Affek et al., 2008), whereas the green  
914 area represents data from fluid inclusion  $\delta D$  (McGarry et al., 2004) – note that  
915 the temperature axis is inverted. B) The correlation between  $\delta^{7}Li$  and palaeo-  
916 temperature for Soreq.



917

918 Figure 8. Silicate weathering congruency, based on calculation of the fraction of  
919 Li in solution relative to that taken into secondary weathering minerals (see text  
920 for details). Significantly more Li is in solution in the interglacials.

921

922

923